Optical coherence tomography measurements of biological fluid flows with picolitre spatial localization

Robert. BYERS [1,] , Stephen J.MATCHER[* 1]

* Corresponding author: Tel.: ++44 (0)114 2225994; Fax: ++44 (0)114 2225945; Email: s.j.matcher@sheffield.ac.uk
[1] Dept of Materials Science & Engineering, Sheffield University, UK

Abstract Interest in studying the human and animal microcirculation has burgeoned in recent years. In part this has been driven by recent advances in volumetric microscopy modalities, which allow the study of the 3-D morphology of the microcirculation without the limitations of 2-D intra-vital microscopy. In this paper we highlight the power of optical coherence tomography (OCT) to image the normal and pathological microcirculation with picolitre voxel sizes. Both Doppler and speckle-variance methods are employed to characterize complex rheological flows both in-vitro and in-vivo. GPU accelerated image registration methods are demonstrated in order to mitigate problems of bulk tissue motion in methods based on speckle decorrelation. In-vivo images of the human nailfold microcirculation are shown.

Keywords: Microcirculation, optical coherence tomography, speckle, phase-sensitive interferometry, rheology

1. Introduction

The human microcirculation is of profound importance to the understanding of many diseases. The sub-mm arterioles, venules and capillaries are the dominant sites of nutrient delivery, waste product removal and flow resistance modulation. The microcirculation also gives rise to important physiological signals such as the BOLD response widely used in functional MRI. Evidence exists that the microcirculatory morphology can be a useful biomarker for conditions such as skin cancer which are otherwise hard to detect with useable sensitivity and specificity. There is thus intense interest in developing new methods to image the microcirculation. The microcirculation has a complex 3-D structure, with strong anatomical variation on spatial scales of tens to hundreds of microns. The smallest vessels are so small that individual red blood cells must deform to pass through them. Flow velocities are typically in the range 0.01 to 1 mm per second. The vascular network geometry is highly non-trivial, so that flows are often oriented at unfavourable angles. Together these restrictions make tough demands on any imaging modality. Optical coherence tomography (OCT) is emerging as a powerful tool that can meet many of these challenges.

OCT is an optical analogue of ultrasound imaging, with limited depth penetration into biological tissues (< 2mm) but offering high spatial resolution (picolitre voxels) and high voxel acquisition rates (up to 1 Gigavoxel per second). First generation time-domain OCT (TD-OCT) was superceded in 2003 by Fourier domain OCT (FD-OCT), bringing a 100-fold improvement in acquisition speed with no SNR penalty. OCT combines readily with Doppler velocimetry to provide 3-D flow mapping with excellent spatial, temporal and velocity resolution.

2 Doppler OCT and Doppler amplitude OCT

First generation time-domain OCT can be given velocity sensitivity by processing the low-coherence interferogram using joint time-frequency techniques such as the short-time Fourier Transform (STFT) [1]. We used this technique to study the rheology of whole

blood in capillary vessels and demonstrated measurements of non-parabolic flow profiles characteristic of biphasic flows. Measuring the amplitude as well as the centre frequency within an STFT window allows mapping of the local concentration of moving scatterers. We used this to demonstrate the phenomenon of red-blood cell "tubular pinch" aggregation at high shear rates in whole blood[2].

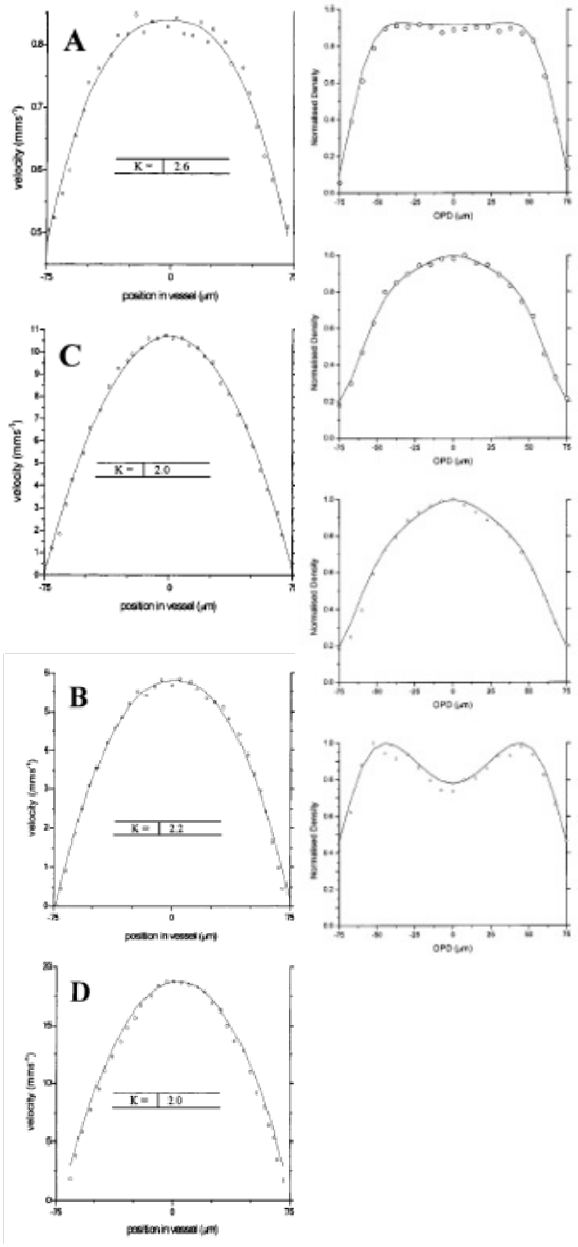

Figure 1 Doppler amplitude OCT scans of human red blood cells flowing in a 150 micron diameter glass capillary tube. Doppler OCT and Doppler amplitude OCT are sensitive to the local velocity and concentration of moving scatterers respectively. The left column shows the characteristic "blunted" non-Poiseuille flow profile produced by red blood cells at low shear rate (A), slowly migrating to Poiseuille-type parabolic profile at high shear (D). The corresponding radial distribution of cells transforms from near-uniform (top-right) to the previously reported "tubular pinch" distribution with a depleted central zone at high shear.

3 Phase-resolved DOCT

STFT analysis leads to an undesirable trade-off between velocity resolution and spatial resolution. This can be overcome by moving to phase-resolved measurements, with the only disadvantage being aliasing at high flow speeds[3]. This can be overcome using high A-scan acquisition rates and/or the method of synthetic phase. The technique can be readily adapted to FD-OCT. We used phase-resolved TD-OCT to demonstrate oscillatory flow dynamics described by Womersley theory in a highly scattering liquid[4] and used phase-resolved FD-OCT to image blood flow in-vivo

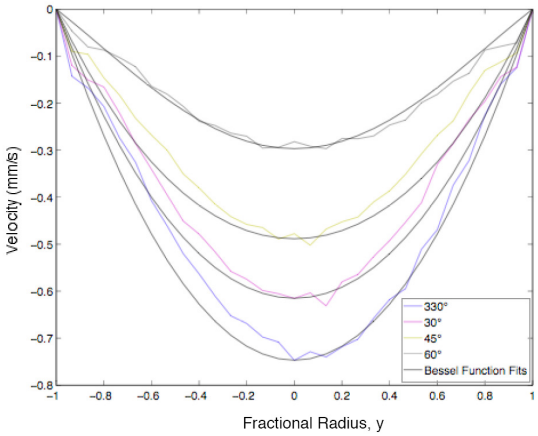

Figure 2. Phase-resolved Doppler OCT scans of oscillatory flow in a glass capillary tube. The velocity precision at fast imaging rates is much improved over STFT-based Doppler OCT, making it feasible to dynamically image evolving flow profiles over the course of a single sinusoidal pressure waveform. Solid lines: fit of the experimental profiles using analytical solutions due to Womersley.

in the cerebral tissue of small animals.

The technique has been very successfully applied to animal and human retinal blood flow imaging, and has great potential in studying neurovascular coupling in the brain, the response of the tumour microcirculation to therapeutic interventions and the presence of non-melanoma and melanoma epithelial cancer.

4 Speckle-variance and correlation mapping OCT

A limitation of phase-resolved FD-OCT is its

sensitivity to motion artefacts. The high B-scan acquisition rates of FD-OCT systems makes dynamic speckle imaging a viable proposal. Speckle-variance OCT is less sensitive to motion artefacts than phase-resolved OCT but lacks quantification of flow velocity. The long acquisition times of speckle-variance imaging can be reduced by correlation-mapping, where the statistics are accumulated over a kernel in the image rather than a pixel time-series[5].
We used correlation-mapping OCT (cm-OCT) to detect the presence of the superficial blood vessels in the human nailfold. Such microangiography applied clinically could offer new ways to detect skin and oral cancer, with improved specificity due to the rejection of confounding influences such as inflammation.

A major clinical challenge regarding the *in-vivo* application of cm-OCT is related to the concept of bulk tissue motion (BTM). This is comprised of in-plane (x-z) and out-of-plane (y-z) shifts resulting from patient movements such as breathing, muscular spasms or the heartbeat. There are two main methods of reducing BTM in acquired *in-vivo* data sets: the first method is to simply increase the imaging frame rate such that any interframe displacements are minimised. The second method involves stabilising the imaging region of interest, through use of restraints or relaxants. Given that *in-vivo* datasets were collected from human volunteers; it wasn't feasible or time efficient to sedate the patients. Instead, care was taken to ensure that seating positions were comfortable and excessive pressure wasn't being applied to the imaging area, a practice that's also advantageous given how easily the microvasculature can become occluded.

Using a 20 kHz swept-source OCT machine (VivoSight - Michelson Diagnostics Ltd), data was acquired from a 2×2×2mm volume of the nail fold. The VivoSight OCT scanner utilises a 1305nm (Centre wavelength) beam that's capable of distinguishing structural morphology down to a resolution of approximately 5µm axial and 7.5µm lateral, with B-scans being acquired at a rate of approximately 20 frames per second. The galvanometer was stepped in the y-direction with a spacing of 1µm, collecting 2000 total B-scans. The 1µm y-spacing was chosen such that changes in interframe tissue morphology were minimised, resulting in a high speckle signal to noise ratio between frames.

It was found that various pre-processing and post-processing methodologies can be applied to speckle-variance datasets in order to improve vasculature contrast and reduce the effects of noise. The 4 channels that are collected simultaneously by the VivoSight OCT machine can be blended together and combined to produce an image with notably reduced shot, thermal and excess photon noise. As speckle is a multiplicative noise source that's caused by the coherent processing of backscattered signals from multiple targets within a voxel; its origins are not random, hence it persists across the blending operation. An instance of the image is then convolved with a 3x3 median filter and used to generate a binary noise mask which suppresses any pixels that don't exceed a calculated noise floor intensity.

The presence of interframe BTM is reduced through use of a sub-pixel accurate phase correlation image registration algorithm. For this, an initial pixel-accurate estimation of x-z shift is optimised using up-sampled discrete Fourier transforms (DFT's) of the area surrounding the correlation peak. This process is far more memory efficient than calculating zero-padded FFT's of the entire image, and was used to achieve an accuracy of $1/100^{th}$ of a pixel. Pre-processing is concluded by the removal of reflective artefacts and noise that are present above the skin surface. The hyperreflective skin surface is detected using a modified Sobel edge detection algorithm. A mask is then generated which removes any noise derived signal that's situated above the skin.

As previously mentioned, a technique known as correlation-mapping OCT was used to generate vasculature contrast. The Pearson's correlation coefficient was compared between adjacent 5x5 kernels, sharing the same x-z location. Absolute correlation values close to 1 implied that the region was solid, as very little temporal variance had occurred. Correlation values close to 0 implied that the region was fluid, as temporal decorrelation had taken place. This method is advantageous in comparison to Doppler-OCT in that the derived contrast is independent of the flow direction, though functional data cannot be extracted at this point.

Internal tissue deformations that were caused by motions such as the heartbeat or breathing weren't effectively eliminated by the image-registration algorithms. This is because the aforementioned algorithms assumed rigid tissue movement, without any deformation.

Realistically the tissue is likely to deform as

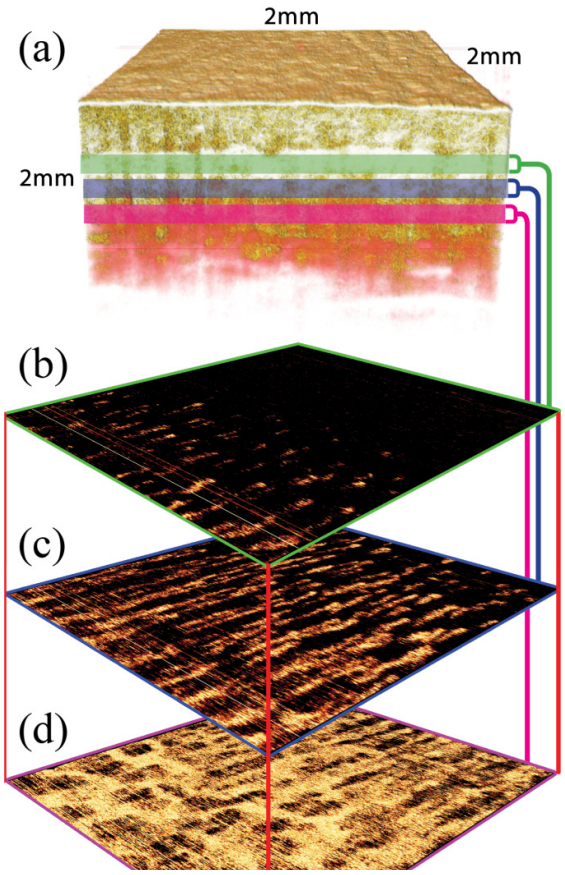

Figure 3 - Correlation-mapping OCT images of the *in-vivo* nail fold. (a) 3D render of the structural B-scan data with maximum intensity projection depths highlighted. (b)(c)(d) Maximum intensity projections of the cm-OCT data across the indicated depths on (a).

the skin expands outwards, causing strong variance measurements at boundaries with large changes in reflectivity, such as the dermal-epidermal junction. Artefacts such as these were attenuated through use of morphological opening and closing operators, a 1-pixel radius disk shaped structuring element was used to eliminate anomalous signal and close any small gaps.

In addition to morphological opening and closing, a step-down exponential filter function was designed in order to reduce the shadowing artefacts present beneath vessels. This simple function uses a convolution operation to sum the intensities of "n" pixels that lie directly above the pixel-of-interest in the depth direction (z). The pixel of interest is then scaled by a factor that's exponentially proportional to the sum of pixel intensities. This process attenuates the artificial signal that's caused by the forward scattering of light by the red blood cells.

These processing steps were then applied to the aforementioned nailfold dataset.

Figure 3(d) displays what appears to be the underlying vasculature plexus that's situated deep within the reticular dermis of the nail fold. As a result of the depth, the image contains relatively large amounts of noise, albeit the distinct curvature of the vasculature is still visible. Figure 3(b) and (c) show the main body and tips of the capillary coils that rise up to provide the papillary dermis with

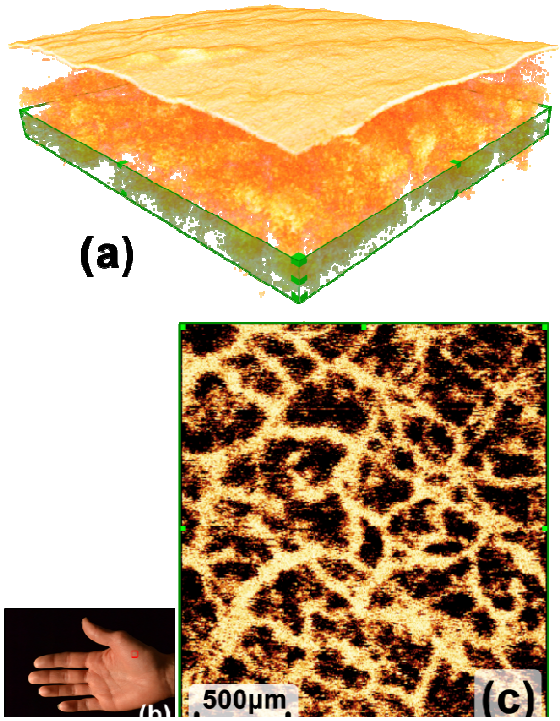

Figure 4 - (a) 3D render of the structural data, green box shows the depth of the maximum intensity projection. (b) Image of the palm - Red box shows imaging region. (c) cm- OCT projection of the reticular dermis.

nutrients.

A second 2x2x2mm data-set was obtained by imaging a region of the lower palm, the results of cm-OCT are shown in figure 4. High vessel density can be seen on cm-OCT images of the palm. In addition, the vasculature plexus is situated within the reticular dermis layer of the skin, in line with current histological knowledge.

To demonstrate the contrast that's derived as a result of cm-OCT, a wide field of view (FOV) region of the ankle was imaged. This consisted of 3000 frames forming a volume of 1.5x3x2mm, a comparison between the structural and cm-OCT data is shown in figure 5. No microvasculature is visible when

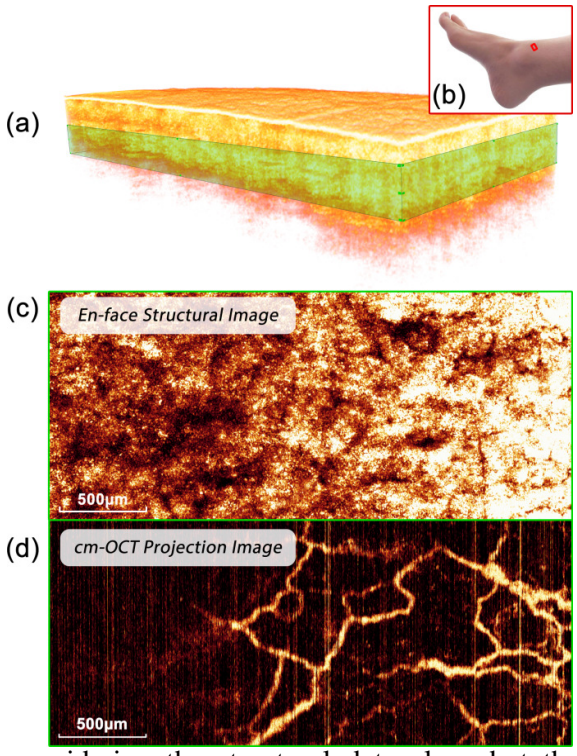

Figure 5 - (a) 3D render of the structural data, green box shows the depth of the maximum intensity projection. (b) Image of the ankle - Red box shows imaging region. (c) En-face structural image taken at the z-midpoint of the green box in (a). (d) cm-OCT maximum intensity projection.

considering the structural data alone but the cm-OCT projection reveals a clear view of vessels down to around 20µm in diameter.

In order to extend the clinical utility of cm-OCT, it would be beneficial to facilitate real-time processing of the speckle-variance data. This would allow the operator to move the scanner across any sites of interest while a real-time view of the microvasculature is updated on the screen. Decisions regarding surgical intervention and diagnosis could be made without subjecting the patient to long waiting times or repeat scans. One method of improving the throughput of the cm-OCT pipeline is related to the concept of parallel processing. That is; breaking down large tasks into smaller, independent tasks that can be computed in parallel.

An emerging method of parallelisation is achieved by modifying algorithms such that they make use of graphical processing unit (GPU) hardware, a process known as: General-Purpose Computing on Graphics Processing Units (GPGPU). This is advantageous in the context of certain algorithms, particularly when considering the difference in architecture between CPU and GPU processors. While CPU's typically contain a small number of high-speed cores (2-8) that are optimised for sequential serial processing tasks, GPU's exhibit thousands of smaller lower-speed cores that are designed specifically to handle multiple tasks in parallel. In addition to this, GPU's are capable of working in tandem with the CPU, so tasks can be allocated to the appropriate hardware as required. There are still limitations related to data transfer overheads, as the GPU can only process data that's stored within its own onboard memory, hence it's beneficial to avoid sending large data sets multiple times between the CPU and GPU hardware.

An Nvidia GTX 780 GPU was used to accelerate the aforementioned cm-OCT pipeline, making use of the Parallel computing toolbox™ (MATLAB 2013b). An overall speed-up of 4.3x was achieved across the entire pipeline, with individual functions being accelerated between 18.9x (Channel blending) and 1.78x (Binary noise mask). An optimised form of the pipeline was accelerated to a throughput of 155.3 frames per second when using a solid-state disk for data loading, this can potentially be improved further by utilising the low level memory control that's offered by a real time (RT) operating systems.

References

[1] Z. Chen, T. E. Milner, S. Srinivas, X. Wang, A. Malekafzali, M. J. C. van Gemert, and J. S. Nelson, ‘‘Noninvasive imaging of in vivo blood flow velocity using optical Doppler tomography,’’ Opt. Lett. **22(14)**, 1119–1121 (1997).

[2] Moger J, Matcher SJ, Winlove CP and Shore AC “Measuring red blood cell flow dynamics in a glass capillary using Doppler optical coherence tomography and Doppler amplitude optical coherence tomography” *J. Biomed. Opt.* **9(5)**, 982-994 (2004).

[3] Zhao YH, Chen ZP, Saxer C, Xiang SH, de Boer JF, Nelson JS, “Phase-resolved optical coherence tomography and optical Doppler tomography for imaging blood flow in human skin with fast scanning speed and high velocity sensitivity”, *Opt. Lett.*, **25**, 144-146 (2000).

[4] C Blake, J Edmunds, L Shelford, J Moger, and SJ Matcher, "Measurement of sinusoidal flow oscillations in a glass capillary tube using phase-resolved DOCT", *Proc. SPIE* **6847**, 68472O (2008)

[5] E. Jonathan, J. Enfield and M. J. Leahy, “Correlation mapping method for generating microcirculation morphology from optical coherence tomography (OCT) intensity images”, *J. Biophotonics* 1–5 (2010).